Supplementary information for:

Bridge improvement work: Maximising Non-Linear Optical Performance in Polyoxometalate Derivatives

Claire F. Jones, Bethany R. Hood, Yovan de Coene, Ivan Lopez-Poves, Benoît Champagne, Koen Clays, and John Fielden

General

Materials and Procedures. Acetonitrile (MeCN) for synthesis, UV-visible spectroscopy and electrochemistry was dried over molecular sieves using an MBraun solvent purification system (SPS). Dry dimethyl sulfoxide (DMSO) and dry dimethyl formaldehyde (DMF) was purchased from Sigma Aldrich (SureSeal) and Acros Organics (AcroSeal). Acetonitrile for Hyper-Rayleigh Scattering (HRS) studies was dried for 48 hours over 3Å molecular sieves and degassed by bubbling through nitrogen. Solutions for UV-visible spectroscopy were filtered through Fisherbrand 0.45µm PTFE syringe filters to remove molecular sieve particulates. All other reagents and solvents were obtained as ACS grade from Sigma Aldrich, Alfa Aesar, Fisher Scientific, Fluorochem, Acros Organics, or Apollo Scientific and used as supplied. Deuterated solvents were obtained from Eurisotop, Cambridge Isotope Laboratories, or Acros Organics and used as supplied. Tetrabutylammonium hexamolybdate[1] was synthesized according to previously published methods. The hexamolybdate derivatization chemistry and preparation of organic precursors was performed under an atmosphere of dry argon or nitrogen using standard Schlenk techniques. Precursor compounds **L1a**,[2a] **L1b**,[2b] **L3a**,[3a] **L3b**,[3b] were all synthesised by established methods, hexamolybdate derivative compound **2** was previously synthesised in our group.[4]

General Physical Measurements. ^{1}H- and ^{13}C-NMR spectra were acquired using Bruker Ascend 500 (500 MHz) and Bruker Ultrashield Plus 400 (400mHz) spectrometers and all shifts are quoted with respect to TMS using the solvent signals as secondary standard (s = singlet, d = doublet, t = triplet, q = quartet, quin = quintet, sex = sextet, hept = heptet, dt = doublet of triplets, m = multiplet). For compound **1** only one out of three quaternary carbon signals were observed for these compounds even after >3000 scans of a saturated solution, which gave strong signal for all non-quaternary ^{13}C resonances. Elemental analyses performed by the University of Manchester Microanalysis laboratory for compound **1** and London Metropolitan University for all other compounds. Negative ion electrospray mass spectrometry was performed by the UK National Mass Spectrometry Service at Swansea University (negative ion nanoelectrospray (nESI) on the Advion nanomate and Thermo LTQ Orbitrap XL) for compound **1** and by the John Innes Centre on a Shimadzu IT-ToF for compound **3**. Due to the number of possible isotopologues for hexamolybdate clusters the mass spectra are broad envelopes and the monoisotopic peak is not observed. This means that the results cannot be considered accurate mass, but theroretical and observed isotopic profiles match and give us confidence that these ions represent the proposed species. UV–Vis spectra were obtained by using an Agilent Cary 60 UV-Vis spectrophotometer.

Synthetic Methods

Our synthetic route to compounds **1** and **3** is shown in Scheme S1.
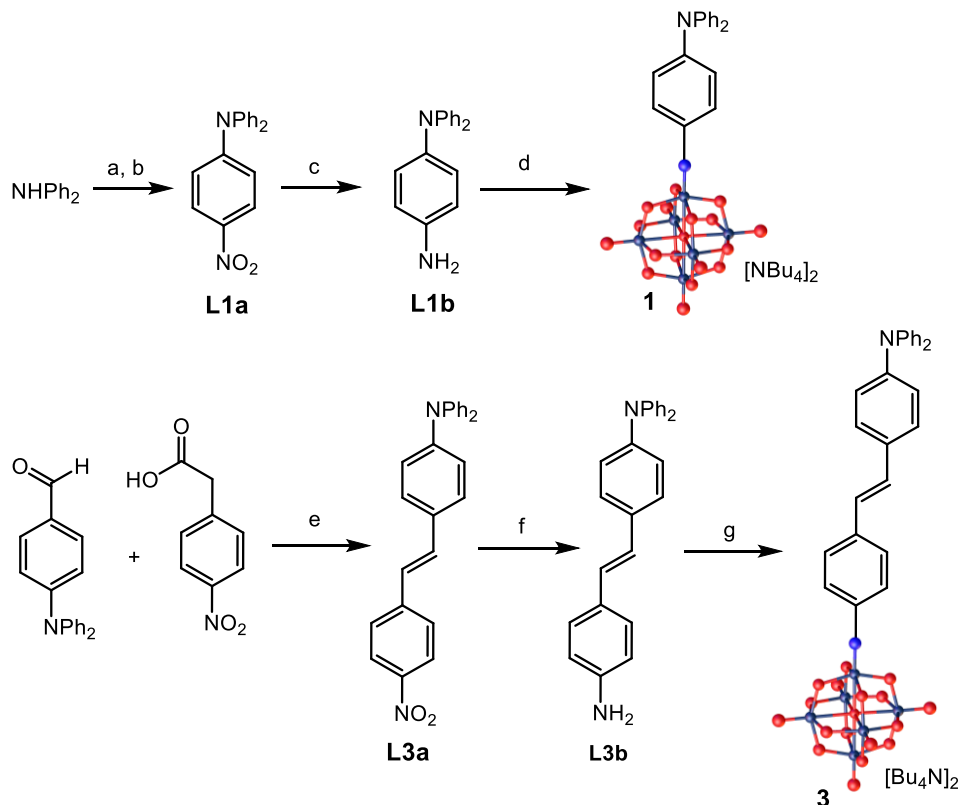
Scheme S1: Synthetic route to compound [**1**] and [**3**]. Reagents and conditions: (a) NaH, DMF, 0 ℃ to RT, 1 h (b) 4-nitro-1-fluorobenzene, 0 ℃, then 110 ℃, 4 h. (c) H_2, 10 mol% Pd/C, MeOH:EtOAc (1:1), 16 h. (d) [NBu$_4$]$_2$[Mo$_6$O$_{19}$], DCC, DMSO, 70 ℃, 10 h .(e) Piperidine, 130 ℃ melt, 6 h. (f) Hydrazine, Pd/C, EtOH reflux, 45 min. (g) [NBu$_4$]$_2$[Mo$_6$O$_{19}$], DCC, DMSO, 70 ℃, 10 h.

Preparation of 4-diphenylamino-1-nitrobenzene (L1a)

Synthesis of **L1a** was adapted from the method of Wang *et al.*[2] Diphenylamine (1.012g, 5.90 mmol) as a solution in DMF (5ml) was added dropwise to a stirred suspension of NaH (0.222 g, 9.26 mmol) in 20 ml DMF at 0 ℃.   The reaction mixture was allowed to warm to room temperature over 1 hour. Then the reaction mixture was again cooled to 0 ℃ and an excess of 4-nitro-1-fluorobenzene was added as a solid in portions. The reaction mixture was heated to reflux at 110 ℃ for 3 – 4 hours.   Once cooled the reaction was quenched with ice cold water (50 ml) with vigorous stirring. The crude product was isolated by Bucher filtration and washed with water before recrystallization from hot ethyl acetate (40 ml) and cooling in the freezer (-17 ℃) to yield bright orange crystals, **L1a** (0.454 g, 2.71 mmol, 46%). ^{1}H-NMR (400 MHz, CDCl$_3$) δ 8.04 (2H, d, J = 8.0 Hz), 7.37 (4H, m), 7.23 – 7.17 (6H, m), 6.92 (2H, d, 8.0 Hz). Atom connectivity was established by single crystal X-ray diffraction, unit cell: 12.9961(5), 13.0411(3), 17.3514(3), orthorhombic, V = 2940.77(14), space group: *Pbca*.

Preparation of 4-diphenylamino-aniline (L1b)   To a mixture of **L1a** (0.263 g, 0.90 mmol)
and Pd/C (0.026 g) under nitrogen was added a degassed mixture of methanol (75 ml) and ethyl acetate (75 ml). The nitrogen atmosphere was substituted for hydrogen using a balloons filled

with hydrogen gas. The reaction was left to stir overnight at room temperature. The Pd/C was removed by filtration through celite and the solvent was removed in vacuo. The crude solid product was precipitated from cold ethyl acetate with hexane and collected by Bucher filtration to give **L1b** (0.112 g, 0.423 mmol, 47%), proton NMR was consistent with that previously reported:[2] ^{1}H-NMR 400 MHz, CDCl$_3$ δ: 7.19 (m, 4H), 7.03 (m, 4H), 6.96 (d, $J = 8.7$ Hz, 2H), 6.91 (m, 2H), 6.65 (2H, d, $J = 8.7$ Hz), 3.62 (2H, s, br).

Preparation of [NBu$_4$]$_2$[Ph$_2$NC$_6$H$_4$NMo$_6$O$_{18}$] (1)

L1b (0.090 g, 0.34 mmol) and [NBu$_4$]$_2$[Mo$_6$O$_{19}$] (0.490 g, 0.36 mmol) were added to a Schlenk tube under argon. In a separate Schlenk tube DCC (0.109 g, 0.60 mmol) was dissolved in anhydrous DMSO (5ml) and the solution was then transferred to the Schlenk tube containing the solid reagents. The reaction mixture was heated with stirring at 70 °C for 10 hours, becoming dark brown after 15 minutes. Once cooled to room temperature the reaction mixture was filtered into a mixture of 68 ml diethyl ether and 18 ml ethanol with vigorous stirring and a dark red precipitate formed. The precipitate was collected by vacuum filtration and washed with the diethyl ether/ethanol mixture (3 × 10 ml) before drying under vacuum yielding **1** as a dark red powder (0.335 g, 0.21 mmol, 59%). ^{1}H NMR (400 MHz, CD$_3$CN): δ 7.24 (d, $J = 9.2$ Hz, 2H), 7.22 (d, $J = 8.2$ Hz, 2H), 7.00 (d, $J = 8.9$ Hz, 2H), 6.98 (m, 6H), 6.82 (d, $J = 8.9$ Hz 2H), 3.34 (m, 16H), 1.71 (quin, $J = 8.0$ Hz, 16H), 1.35 (sex, $J = 7.4$ Hz, 16H), 0.87 (t, $J = 7.4$ Hz, 24H). ^{13}C NMR (100.62 MHz, CD$_3$CN): δ 148.73, 147.74, 130.61, 128.42, 126.39, 121.50 59.30, 24.38, 20.35, 13.86. Anal. Calcd (found) % for C$_{53}$H$_{88}$Mo$_6$N$_4$O$_{18}$: C 37.37 (37.41), H 5.39 (5.38), N 3.49 (3.43). m/z = 1363.74 [(NBu$_4$)[C$_{18}$H$_{14}$N$_2$Mo$_6$O$_{18}$]]$^-$, 560.73 [C$_{18}$H$_{14}$N$_2$Mo$_6$O$_{18}$]$^{2-}$. FTIR (KBr): 2961 (m), 2935 (sh), 2873 (m), 1580 (s), 1488 (s), 1380 (w), 1332 (m), 1316 (m), 1283 (m), 1169 (w), (vw), 974 (m), 950 (s), 879 (vw).

Preparation of 4-(4-nitrophenylethenyl)-N,N-diphenylaniline (L3a)

Synthesis of **L3a** was based on the method of Ding et al.[3a] A mixture of 4-nitrophenyl acetic acid (1.629 g, 8.99 mmol), 4- diphenylaminobenzaldehyde (0.820 g, 3.00 mmol), and piperidine (0.9 ml, 9.11 mmol) in a Ace glass pressure tube was heated to 130 °C with stirring for 6 hours using a Buchi TO-51 glass titrator oven in a vertical stance. At the end of the reaction, excess diphenyaminobenzaldehyde was removed by sublimation, leaving a red residue which was partially dissolved in hot ethanol (50 ml) and filtered through a syringe filter to remove insoluble impurities. The filtrate was concentrated in vacuo until a precipitate began to form, and then the flask was placed in an ice bath and **L3a** was isolated by filtration as a red solid (0.670 g, 1.71 mmol, 57%). ^{1}H-NMR (500 MHz, (CD$_3$)$_2$SO) δ 8.21 (d, $J = 8.9$ Hz, 2H), 7.82 (d, $J = 8.9$ Hz, 2H), 7.57 (d, $J = 8.8$ Hz, 2H), 7.48 (d, $J = 16.4$ Hz, 1H), 7.34 (dd, $J = 8.5$, 7.4 Hz, 4H), 7.26 (d, $J = 16.4$ Hz, 1H), 7.10 (tt, $J = 7.5$, 1.1 Hz, 2H) 7.07 (dd, $J = 7.4$, 1.1 Hz, 4H), 6.96 (d, $J = 8.8$ Hz, 2H).

Preparation of 4-(4-aminophenylethenyl)-N,N-diphenylaniline (L3b)

Synthesis of **L3b** was based on the method of Lu et al.[3b] **L3a** (0.350g, 0.890 mmol) was dissolved in anhydrous degassed ethanol (12 ml). Pd/C (0.012 g) was added followed by 10 equivalents of hydrazine monohydrate (0.40 ml, 8.90 mmol). The reaction mixture was refluxed for 45 minutes and then filtered hot using a filter cannula. Upon cooling, yellow solid

L3b (0.202 g, 0.558 mmol, 63%) was recovered by filtration. ^{1}H-NMR (500 MHz, $(CD_3)_2SO$) δ 7.41 (d, J = 8.6 Hz, 2H), 7.30 (dd, J = 8.5, 7.3 Hz, 4H), 7.24 (d, J = 8.6 Hz, 2H), 7.06–6.98 (m, 6H), 6.96–6.91 (m, 3H), 6.84 (d, J = 16.4 Hz, 1H), 6.55 (d, J = 8.5 Hz, 2H) 5.27 (s, 2H).

Preparation of [NBu4]2[Ph2NC6H4CHCHC6H4NMo6O18] (3)

Tetrabutylammonium hexamolybdate (0.499 g, 0.366 mmol), compound **L3b** (0.126g, 0.348 mmol), and DCC (0.086 g, 0.417 mmol) were dissolved in 5 ml of anhydrous dimethylsulfoxide, and the resulting yellow solution heated at 70ºC for 10 hours. When cool, a pale yellow precipitate was removed by filtration and the solution precipitated by slow addition to a mixture of 75 ml of diethyl ether and 12 ml of ethyl acetate. The resulting solid was collected by filtration, washed with ethyl acetate and diethyl ether to give crude compound **3** (0.414 g). Integration of the tetrabutylammonium ^{1}H-NMR peaks vs the aromatic region indicated the crude material was *ca.* 30% $[NBu_4]_2[Mo_6O_{19}]$. Purification was achieved by reprecipitation from acetonitrile using diethyl ether, extraction of the precipitate with DCM, and removal of the DCM in vacuo before a final reprecipitation by diffusion of diethyl ether into acetone, yielding compound **3** as a dark red solid (0.030 g, 0.018 mmol, 5%). ^{1}H NMR (500 MHz, CD_3CN) δ 7.55 (d, J = 8.4 Hz, 2H), 7.46 (d, J = 8.9 Hz, 2H), 7.31 (m, 4H), 7.22 (d, J = 8.4 Hz, 2H), 7.18–7.06 (m, 8H), 6.99 (d, 2H, J = 8.8 Hz), 3.08 (m, 16H), 1.60 (quin, J = 8.0 Hz, 16H), 1.35 (sex, J = 7.3 Hz, 16H), 0.97 (t, J = 7.4 Hz, 24H). ^{13}C-NMR (100.62 MHz, CD_3CN) δ 154.41, 148.84, 148.38, 138.80, 131.93, 131.09, 130.47, 128.80, 127.50, 127.21, 126.31, 125.60, 124.45, 123.74, 59.30, 24.38, 20.35, 13.86. Anal. Calcd (found) % for $C_{58}H_{92}N_4O_{18}Mo_6$: C 40.76 (40.26), H 5.43 (5.35) N 3.28 (3.21). m/z = 1223.51 $[(H)[C_{26}H_{20}N_2Mo_6O_{18}]^-$, 611.76 $[C_{26}H_{20}N_2Mo_6O_{18}]^{2-}$. FTIR (ATR): 2961 (m), 2933 (sh), 2873 (m), 1580 (m), 1507 (m), 1484 (m), 1379 (w), 1327 (m), 1315 (sh), 1276 (m), 1175 (vw), 1154 (vw), 1104 (vw), 1072 (vw), 1029 (vw), 974 (m), 945 (s), 879 (vw), 839 (vw), 773 (s), 695 (w).

NOTE: Despite many attempts, a crystalline sample of **3** could not be obtained. Data reported above are for the highest quality material, yet the elemental analysis is consistent (to within 0.07% on C, H and N) for a 5 mol % impurity of $[NBu_4]_2[Mo_6O_{19}]$ and a peak for $[Mo_6O_{19}]^{2-}$ is visible in the cyclic voltammogram. The 95% pure material was used for UV-vis and 1064 nm HRS measurements. 1200 nm HRS measurements were carried out with a lower purity sample of **3**, with concentrations adjusted for presence of NLO-inactive $[Mo_6O_{19}]^{2-}$.

X-ray Crystallographic Details

Sample Growth, Data Collection and Refinement. X-ray quality crystals of [**1**]·3MeCN were grown by recrysallisation from hot acetonitrile. Data were collected on a Rigaku XtalLab Synergy S diffractometer using a Photon-Jet Cu microfocus source and Hypix hybrid photon counting detector. Data reduction, cell refinement and absorption correction were carried out using Rigaku CrysAlisPro,[5] and the structure was solved with SHELXT[6] in Olex2 V1.5.[7] Refinement was achieved by full-matrix least-squares on all F_0^2 data using SHELXL (v. 2018-

3),[8] also in Olex 2 V1.5. The asymmetric unit contains the complete molecular anion, both tetrabutylammonium cations and three (disordered) MeCN solvent molecules (see Figure S1). Disorder on two tetrabutylammonium side chains was modelled requiring application of restraints to bond distances and thermal parameters. The crystal structure of compound **2** was previously published (CCDC 1837405).[4]

Table S1: Crystallographic Data and Refinement Details for [**1**]·3MeCN

	1
Formula	$C_{56}H_{95}Mo_6N_7O_{18}$
M	6875.27(12)
crystal system	monoclinic
space group	$P2_1/c$
a/Å	12.4406(1)
b/Å	29.2646(3)
c/Å	18.9032(2)
α/deg	90
β/deg	92.5480(1)
γ/deg	90
V/Å^3	6875.27(1)
Z	4
Radiation	Cu Kα ($\lambda = 1.54184$ Å)
T/K	100.00(1)
μ/mm^{-1}	9.273
Cryst. size/mm	$0.159 \times 0.043 \times 0.042$
Cryst. description	Orange plate
No. reflns collected	13558
No. of indep. reflns (R_{int})	13558 [R(int) = 0.0457, R(sig) = 0.0375]
$2\theta_{full}$/deg (completeness)	5.57 to 154.2 (99.6%)
$2\theta_{max}$/deg (completeness)	5.57 to 133.9 (93.2%)
Reflections with $I > 2\sigma(I)$	11462
Goodness-of-fit on F^2	1.070
final R_1, wR_2 [$I > 2\sigma(I)$]^a	R1 = 0.0469, wR2 = 0.1224
(all data)	R1 = 0.0558, wR2 = 0.1274
Peak and hole/e Å^{-3}	1.16 and -1.04

Structures and Selected Bond Lengths. A representation of the asymmetric unit of [NBu$_4$]$_2$[**1**]·3MeCN is shown in Figure S2. Selected bond lengths and angles for the anion [**1**]$^{2-}$ are collected in Tables S2 and S3. The structures show the typical imido-Lindqvist pattern of a shortened bond length from the imido-Mo (Mo^{im}) to the central oxygen (O^c), lengthened equatorial bond lengths from Mo^{im} to the oxygens bridging to the belt Mo positions (Mo^b), and a lengthened axial bond length from the *trans*-Mo (Mo^t) to O^c. Compared to the -NMe$_2$ analogue (**1NMe$_2$**, see reference 7b, main paper) bond distances within the imido-aryl ligands indicate a substantially less quinoidal structure (i.e. less effective donation from N to POM, borne out by electrochemical measurements) in [**1**]$^{2-}$, as shortening of the *ortho*-to-*meta* C-C bond distances vs *meta*-to-*para* is almost negligible. This is a result of delocalisation of the N-lone pair onto the two phenyl groups.
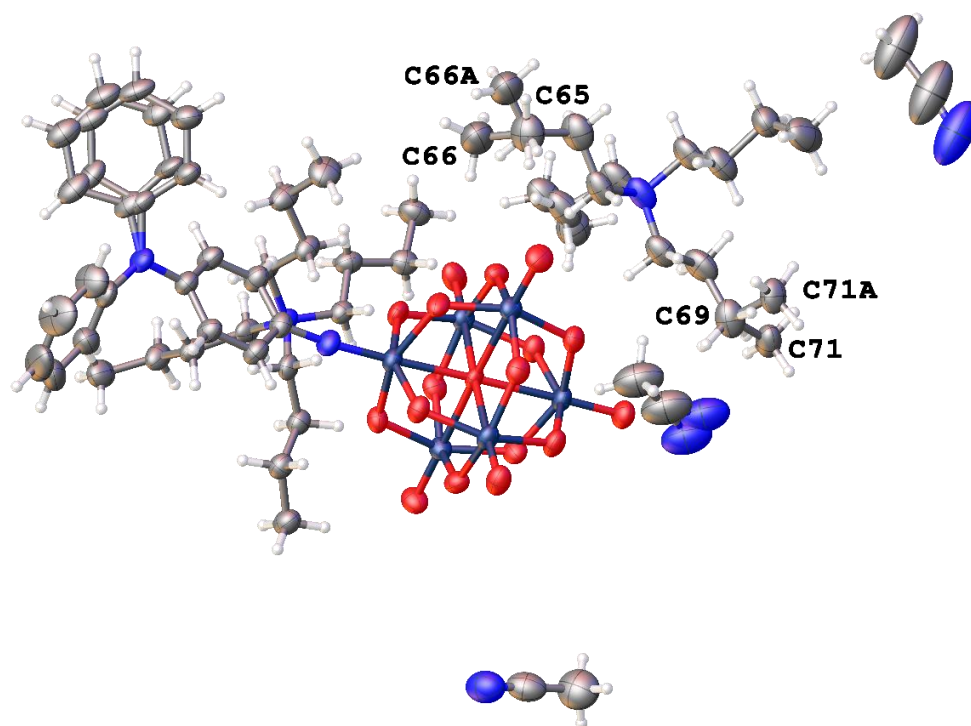
Figure S1: Representation of the asymmetric unit in [NBu$_4$]$_2$[**1**]·3MeCN. Thermal ellipsoids are at the 30% probability level. Disorder of one of the phenyl rings is shown as is disorder of two terminal methyl groups of one of the tetrabutylammonium cations. One of the acetonitrile solvent molecules is also disordered and consisent with three molecules of MeCN in the asymmetric unit. Colour scheme: Mo is navy; O, red; C, gray; N, blue; H atoms are represented by white spheres of arbitrary radii.

Table S2: Selected bond lengths (Å) and angles (°) of the {Mo$_6$} units in anions [**1**]$^{2-}$. Mo^{im} – imido bearing Mo; Mo^b belt Mo; Mo^t, *trans*-Mo; O^c, central O; O^b, bridging O.

	Mo^{im}-N	Mo^{im}-O^c	Mo^{im}-O^b (average)	Mo^t-O^c	Mo^t-O^b (average)	O^c-Mo^{im}-N	Mo^{im}-N-C
1	1.746(4)	2.210(3)	1.952(4)	2.362(3)	1.920(4)	177.78(17)	174.3(4)

Table S3: Bond lengths in the arylimido groups of the anion in **1** compared to **Me$_2$N-1** showing the much less quinoidal structure induced by connection to the electron withdrawing POM in **1**.

$$\left[R_2N \overset{r_1}{\underset{r_2}{\diagdown}} \overset{}{\bigcirc} \overset{r_5}{\underset{r_4}{\diagup}} NMo_6O_{18} \right]^{2-}$$
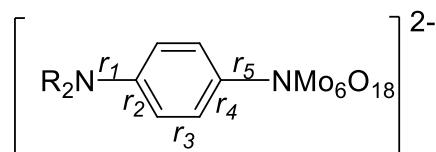
	r_1	$r_2{}^a$	$r_3{}^a$	$r_4{}^a$	r_5
1 (R = Ph)	1.401(6)	1.396(7)	1.381(7)	1.396(8)	1.371(6)
Me$_2$N-1 (R = Me)^b	1.375(5)	1.421(6)	1.355(6)	1.407(5)	1.383(5)

^{a}Average of two C-C bonds bonds in the aryl ring. ^{b}Previously published in ref 7b, main paper.
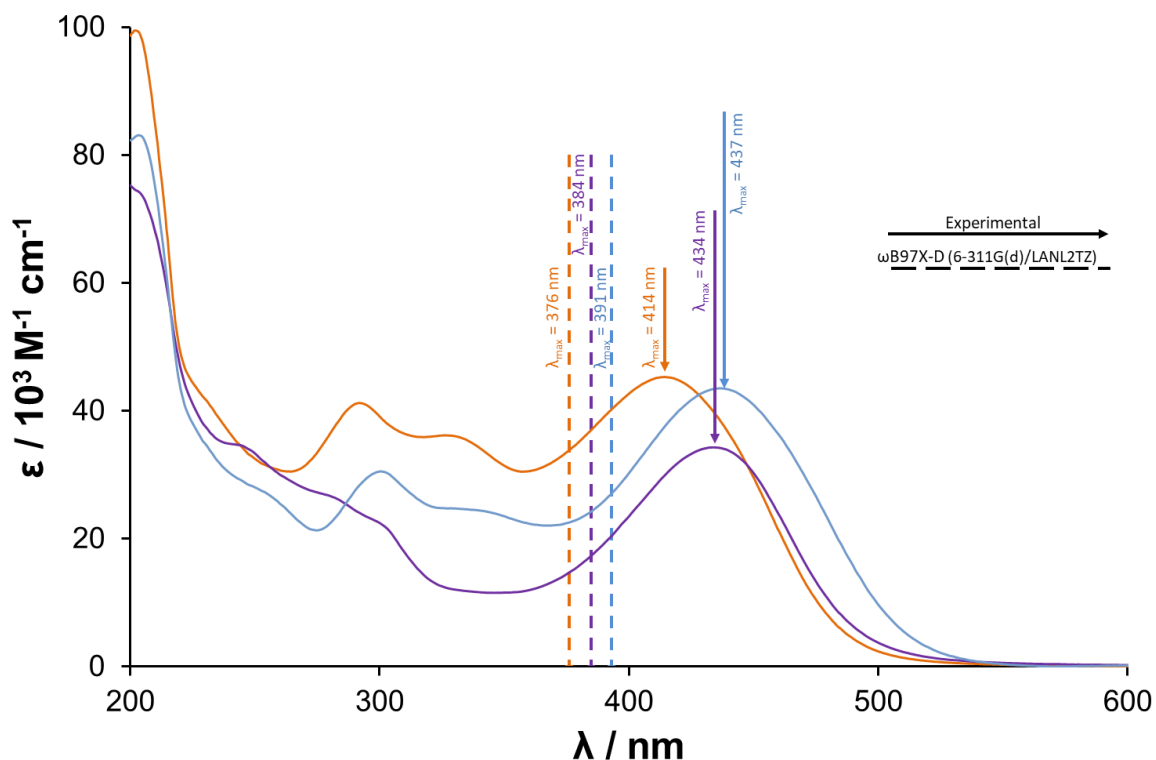
UV-Visible Spectroscopy

Figure S2: Experimental UV-visble spectra of [NBu$_4$]$_2$[**1**], [NBu$_4$]$_2$[**2**] and [NBu$_4$]$_2$[**3**] in acetonitrile.

Electrochemistry

Cyclic Voltammetry. All measurements were carried out using Autolab PGStat 302 potentiostat/galvanostat. A single-compartment three-electrode cell was used with an Ag wire pseudo reference electrode, glassy carbon working electrode and Pt wire auxiliary electrode. [N(C$_4$H$_9$-n)$_4$]BF$_4$,[9] was used as the supporting electrolyte. Solutions containing ca. 10^{-3} M analyte (0.1 M electrolyte) were degassed by purging with argon and blanketed with a continuous flow of argon throughout the experiments. $E_{1/2}$ values (see main text) were calculated from $(E_{pa} + E_{pc})/2$ at a scan rate of 100 mV s^{-1} and referenced to Fc/Fc$^+$.
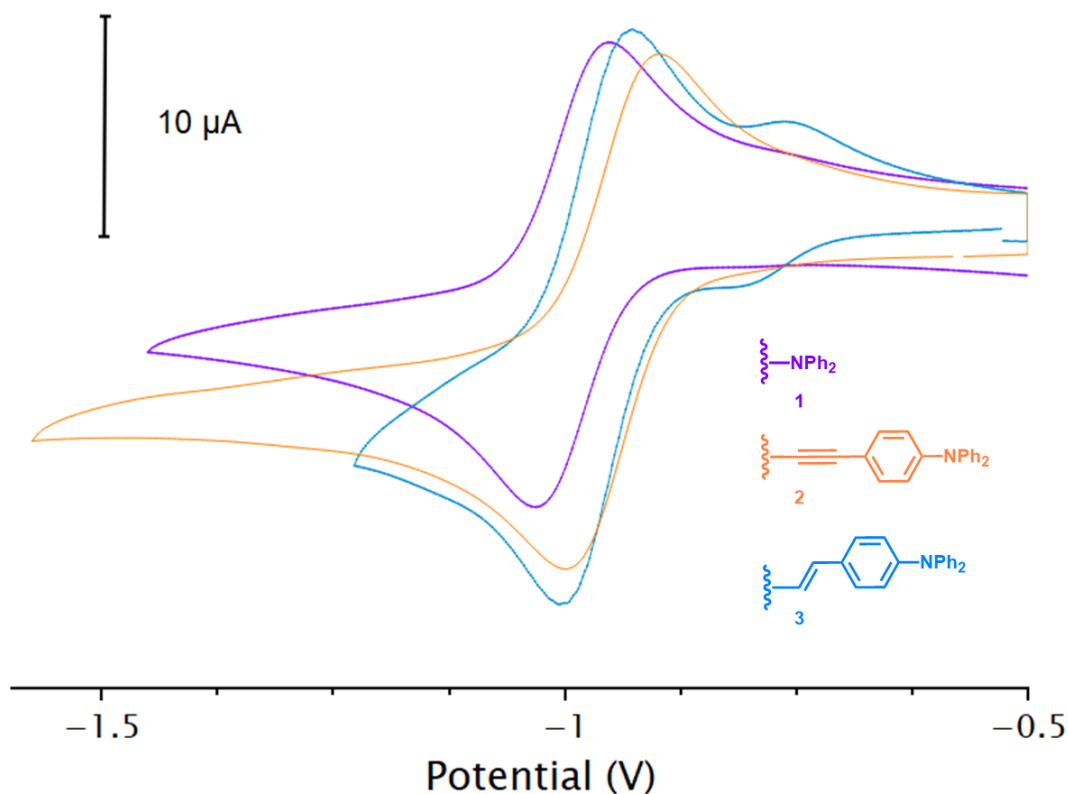
Figure S3: Cyclic voltammograms of **1**, **2** and **3** showing the reversible POM reduction peaks (all *vs* Fc/Fc+). Scan rate 100 mV s-1, GC working electrode, 0.1 M [NBu4][BF4] in acetonitrile as electrolyte. The additional peak in **3** results from residual [Mo6O19]2- which could not be removed, even with multiple reprecipitations and crystallisation attempts. Peak currents are consistent with *ca.* 10%, while elemental analysis fits well for 5% [Mo6O19]2-.

Quantum chemistry calculations

Geometry optimizations. Full geometry optimizations were performed at the density functional theory (DFT) level using the ωB97X-D exchange-correlation functional (XCF).[10] This range-separated hybrid functional combines a modified B97 exchange functional[11] for short-range interactions (from 78 to 0%) with HF exchange for long-range interactions (from 22 to 100%), using the default range-separating parameter, $\omega = 0.2$ Bohr^{-1}. Correlation is described by the B97 correlation functional,[12] and empirical atom-atom London dispersion corrections are included as well. For the C, H, N, and O atoms, the atomic basis set consists of 6-311G(d,p)[13] while LANL2TZ[14] is used for the Mo atoms. TIGHT convergence thresholds on the residual forces on the atoms (1.5 x 10-5 Hartree/Bohr or Hartree/radian) were applied. The reliability of the ωB97X-D/6-311G(d,p)/LANL2TZ method for the geometry optimization of POM derivatives was demonstrated in comparison with other XC functionals in a previous work.[15] To describe the solvent effects (acetonitrile), geometry optimizations were performed in solution using the integral equation formalism (IEF) of the polarizable continuum model (PCM) (IEF-PCM), which represents the solvent by a dielectric continuum characterized by its dielectric permittivity ($\varepsilon_0 = 35.688$ for acetonitrile).[16]

8

Properties of the excited states. Using the optimized geometries, the time-dependent density functional theory (TD-DFT) method[17] with the same XCF, basis set, and IEF-PCM scheme was used to characterize the (lowest-energy) excited states, considering their vertical excitation energies, $\Delta E_{ge} = E_e - E_g$ (from the ground state g to the excited state e), the corresponding transition dipole moment, μ_{ge}, which is related to the oscillator strength, $f_{ge} = \frac{2}{3} \Delta E_{ge} \mu_{ge}^2$, and the difference of dipole moment between states g and e, $\Delta\mu_{ge} = \mu_e - \mu_g$. The excited state dipole moments were calculated by using the nonequilibrium IEF-PCM solvation approach (ε_∞ = 1.807 for acetonitrile). Nonequilibrium solvation TDDFT calculations also provided the difference of electron density between the excited and the ground states, $\Delta\rho(\vec{r}) = \rho_e(\vec{r}) - \rho_g(\vec{r})$. Following Le Bahers *et al*,[18] the barycenters of the positive $[\Delta\rho^+(\vec{r})]$ and negative $[\Delta\rho^-(\vec{r})]$ electron density variations were calculated and the distance between them defines the charge-transfer distance (d_{CT}) while the integration over the whole space of $\Delta\rho^+(\vec{r})$ [or $\Delta\rho^-(\vec{r})$] gives the amount of charge transferred (q_{CT}). The product of these two quantities, $q_{CT} \times d_{CT}$, gives $\Delta\mu_{ge}$. For the oxidized form (closed-shell species), the 120 lowest excitation energies (and oscillator strengths) were calculated.

First hyperpolarizabilities. Using again the same optimized geometries, the SHG β tensor components were evaluated by employing the quadratic response TD-DFT method[19,20] with the same basis set, XCF, and solvation model as for the excited states calculations. Both static and dynamic (incident wavelength of 1064 nm and 1200 nm) responses were calculated. Computing β of large compounds, including those having donor and/or acceptor substituents, is a challenge for TD-DFT because of the intrinsic nonlocal nature of the response and the approximate XCFs (potential and kernel).[21] However, ωB97X-D is a reliable XCF for calculating the β tensors owing to its substantial amount of long-range HF exchange, as demonstrated in previous investigations where the performance of DFT XCFs was assessed with respect to benchmark wavefunction methods.[22-24] Ref. 15 has also evidenced that using local XCFs or XCFs with small amount of HF exchange leads to overestimated first hyperpolarizabilities. The unit sphere representation (USR) was adopted[25] to visualize the β tensors. First, the induced electric dipole moments

$$\vec{\mu}_{ind} = \overset{\leftrightarrow}{\vec{\beta}} : \vec{E}^2(\theta, \phi) \tag{3}$$

are evaluated, where $\overset{\leftrightarrow}{\vec{\beta}}$ is the first hyperpolarizability tensor and $\vec{E}(\theta, \phi)$ is a unit vector of electric field, of which the polarization is defined by the θ and ϕ angles (spherical coordinates). Then, the induced dipoles are plotted on a sphere centered on the molecule center of mass. This allows highlighting the directions along which the second-order polarizations are the strongest (i.e. the largest induced dipoles), its orientation (the acceptor-donor direction).

The method for β calculations accounts for the frequency dispersion of the β response but not for the fact that the UV/visible absorption band has a finite bandwidth. In these TD-DFT calculations the bandwidth is assumed to be zero. Far from resonance, this effect is negligible but when the SHG wavelength falls within the absorption band the impact has to be taken into account. First, the TD-DFT values ($\lambda = 1064\ nm$) were extrapolated by using the simple TSA with a zero bandwidth. Then, these static values are multiplied by a frequency-dependent term

that accounts for the shape of the UV/visible absorption spectrum, following the homogeneous broadening model proposed by Campo *et al.*[26,27] This factor also corrects the overestimation of the calculated vertical excitation energies in comparison to the maximum absorption energies.

Computer codes. All DFT and TD-DFT calculations were performed using the Gaussian16 package.[28] Then, the molecular structures and electron densities were generated using GaussView. The USR pictures, the electron density difference plots, and the simulated UV/vis absorption spectra were generated using the DrawMol software.[29]

TD-DFT UV/visible absorption. The absorption spectrum of [**1**], [**2**] and [**3**] (Figure S5) present bands peaking at 384 nm, 376 nm and 391 nm respectively originating from a single charge-transfer excitations ([**1**] 3.22 eV, f = 1.18, [**2**] 3.30 eV, f = 2.43 and [**3**] 3.17 eV, f = 2.40) and all have far less intense broad bands having maxima at ~290 - 300 nm, associated with many electronic transitions. The fact that the calculated spectrum is shifted to the blue with respect to experiment was expected since the calculations report vertical excitation energies, which do not account for the geometry relaxation of the excited state, neither for the vibronic structure.[30] The presence of a higher-energy band close to 250 nm is also in agreement with experiment, though a closer match would have been achieved by including even more excited states in the TD-DFT calculations.
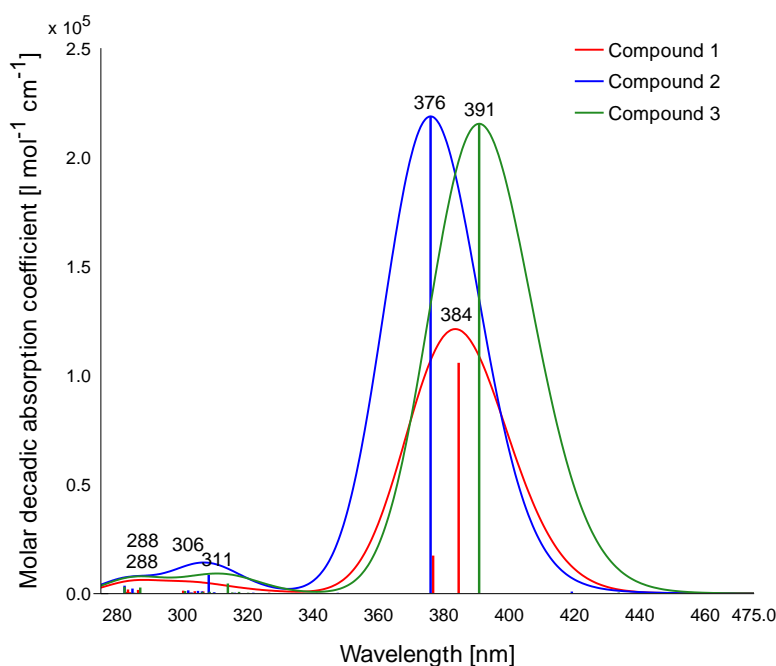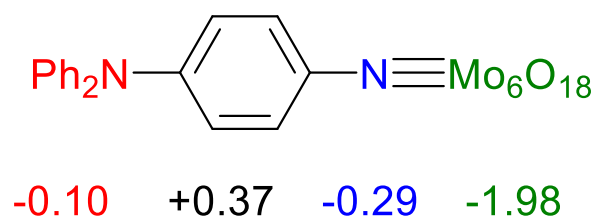

Figure S4: Absorption spectra of the compounds **1**-**3** as calculated at the IEFPCM(solvent = acetonitrile) TDDFT/ωB97X-D/6-311G(d)/LanL2TZ level of approximation. FWHM = 0.3 eV. 30 excited states have been calculated.

Ph_2N — [benzene ring] — $N\equiv Mo_6O_{18}$

-0.10   +0.37   -0.29   -1.98

Compound 1

Ph_2N — [benzene ring] — ≡ — [benzene ring] — $N\equiv Mo_6O_{18}$

-0.12   +0.15   0.00   +0.20   -0.31   -1.92

Compound 2

Ph_2N — [benzene ring] — = — [benzene ring] — $N\equiv Mo_6O_{18}$

-0.14   +0.15   +0.04   +0.20   -0.30   -1.94
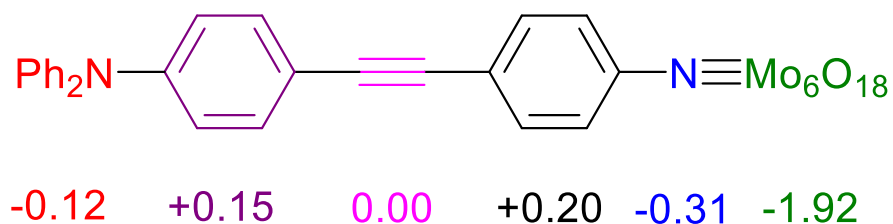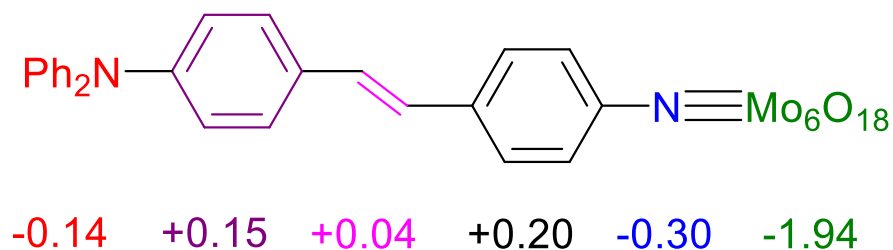
Compound 3

Figure S5: Natural population analysis charges summed for different groups of the chrompphoric anions in **1** to **3**. For clarity groups are colour coded and relevant charges are written directly under the group. As calculated at the IEFPCM(solvent = acetonitrile) DFT/ωB97X-D/6-311G(d)/LanL2TZ level of approximation.

Figure S6: Change of electron density $\Delta\rho = \rho_e - \rho_g$ between the ground and dominant low-energy excited stat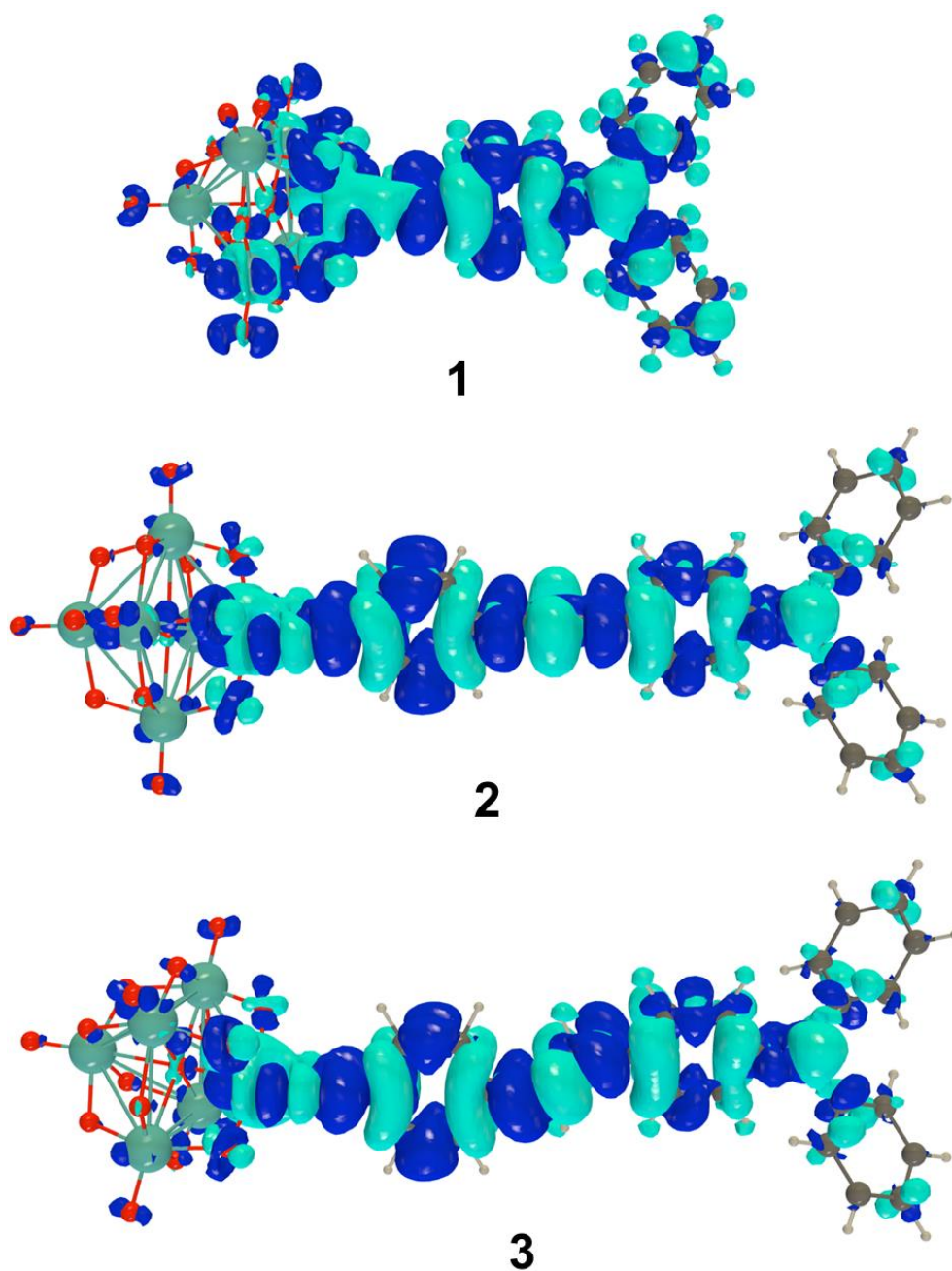es for **1** to **3**, calculated at the IEFPCM(solvent = acetonitrile) TDDFT/ωB97X-D/6-311G(d)/LanL2TZ level of approximation (isovalue = 0.0005 au). Light/dark blue corresponds to negative/positive $\Delta\rho$ so that the excitation induced electron transfer goes from light to dark blue.

Table S4: UV/visible spectra characteristics of compounds **1**-**3** as determined at the ωB97X-D/6-311G(d)/LanL2TZ/IEFPCM(acetonitrile) level of approximation. The β_{HRS} and β_{HRS} quantities have been evaluated using the two-state approximation (in 10^3 a.u.) and the (static) CPKS β_{HRS} values are also given for comparison. (2.5418 D = 1 a.u. of dipole moment; $\beta_{HRS} = \sqrt{\frac{6}{35}}\beta_{zzz} \approx 0.414\,\beta_{zzz}$)

	ΔE (λ) [nRoot]	f^a	d_{CT} (Å)^b	q_{CT} (e)^c	$\Delta\mu$ (D)^d	$\beta_{zzz}^{TSA} = 9\dfrac{f\,\Delta\mu}{\Delta E^3}$	β_{HRS}^{TSA}	β_{HRS}^{CPKS}
1	3.22 (385) [2]	1.18	3.54	0.75	12.8	32.3	13.4	13.9
2	3.30 (376) [2]	2.43	4.34	0.62	12.9	62.2	25.8	16.7
3	3.17 (391) [2]	2.40	4.33	0.62	12.8	68.8	28.5	18.4

^{a} Oscillator strength. ^{b} Charge transfer distance. ^{c} Charge transferred, electrons. ^{d} Ground-to-excited state dipole moment change.

Hyper-Rayleigh Scattering (HRS)

Measurement of HRS. General details of the hyper-Rayleigh scattering (HRS) experiment have been discussed elsewhere,[31] and the experimental procedure and data analysis protocol used for the fs measurements used in this study were as previously described.[32] Measurements were carried out in acetonitrile dried over activated 3Å molecular sieves, and degassed with N_2. The solutions were dilute (*ca.* 10^{-5} M) and filtered (Millipore, 0.45 μm), such that self-absorption of the SHG signal was negligible, verified by the linear relation between signal and a series of five concentrations. UV-vis spectra before and after HRS indicated no noticeable decomposition resulting from two photon absorption. The 1064 nm and 1200 nm source was a Spectra-Physics InSight® DS+ laser (1W average power, sub-100 fs pulses, 80 MHz). In this setup, the collection optics are coupled to a spectrograph (model Bruker 500is/sm), together with an EMCCD camera (Andor Solis model iXon Ultra 897). Correction for multiphoton induced fluorescence was done by subtracting the broad MPF background signal from the narrow HRS peak (FWHM ± 9 nm). The high accuracy of this setup enables us to use the solvent as an internal reference (acetonitrile, $\beta_{HRS,1064} = 0.258 \times 10^{-30}$ esu; $\beta_{zzz,1064} = 0.623 \times 10^{-30}$ esu).[33] For consistency, the B convention is used to report all β values, both experimental and computational.

Table S5 below presents the results for **1** to **3** at both wavelengths, together with the nitro analogue of **3**, (**3-NO₂**) and relevant POM and -NO$_2$ comparisons from our previous work.

Table S5: 1064 nm and 1200 nm HRS data of compounds presented in this paper, and relevant POM and -NO_2 comparisons from our previous work.

Number / Structure (all POM anions are NBu_4^+ salts)	λ_{max}	$\beta_{zzz, 1064}{}^{a}$	$\beta_{zzz, 1200}{}^{a}$	$\beta_{0, zzz}{}^{b}$ (1064)	$\beta_{0, zzz}{}^{b}$ (1200)	$\beta_0/N^{3/2\,c}$
	/ nm	/ 10^{-30} esu				
1[d] $\left[Ph_2N\text{—}\bigcirc\text{—}NMo_6O_{18} \right]^{2-}$	434	-	430±30	-	180±10	12.2
2[d,e] $\left[Ph_2N\text{—}\bigcirc\text{—}\equiv\text{—}\bigcirc\text{—}NMo_6O_{18} \right]^{2-}$	414	590±20	376±30	196±7	174±10	3.32
3[d] $\left[Ph_2N\text{—}\bigcirc\text{—}=\text{—}\bigcirc\text{—}NMo_6O_{18} \right]^{2-}$	437	1040±20	640±30	281±7	260±10	4.96
3-NO_2[d] $Ph_2N\text{—}\bigcirc\text{—}=\text{—}\bigcirc\text{—}NO_2$	420	-	451±40	-	202±18	3.86
Me_2N-1[f] $\left[Me_2N\text{—}\bigcirc\text{—}NMo_6O_{18} \right]^{2-}$	424	283±7	-	87±2	-	5.90
Me_2N-2[f] $\left[Me_2N\text{—}\bigcirc\text{—}\equiv\text{—}\bigcirc\text{—}NMo_6O_{18} \right]^{2-}$	421	440±55	-	139±17	-	2.65
Me_2N-1-NO_2[f] $Me_2N\text{—}\bigcirc\text{—}NO_2$	394	84±13	-	33±5	-	2.17
Me_2N-2-NO_2[f] $Me_2N\text{—}\bigcirc\text{—}\equiv\text{—}\bigcirc\text{—}NO_2$	406	452±68	-	161±24	-	3.08

[a] β_{zzz} calculated assuming a single dominant tensor component, measured using 1064 or 1200 nm fundamental laser beams. The quoted units (esu) can be converted into SI units (C^3 m^3 J^{-2}) by dividing by a factor of 2.693×10^{20}. [b] Non-resonant, static β estimated from $\beta_{zzz, 1064}$ or $\beta_{zzz, 1200}$ using the two state model. [c] N = Number of electrons in π-bridge. [d] This work. [e] Ref. 4. [f] Ref. 7b, main paper.

References

1. W. G. Klemperer, *Inorg. Synth.* **1990**, *27*, 71.

2. (a) K-L. Wang, T-S. Tseng, H-L. Tsai, S-C. Wu, *J. Polymer Sci: Part A.*, **2008**, *46*, 6861

3. (a) G. Ding, Y. Lu, X. Qin, J. Su, S. Zhang, H. Li, Z. Luo, L. Chen, F. Gao, *Dyes Pigm.* **2017**, *139*, 19–32. (b) X. Lu, G. Zhang, D. Li, X. Tian, W. Ma, S. Li, Q. Zhang, H. Zhou, J. Wu, Y. Tian, *Dyes Pigm.* **2019**, *170*, 107641.

4. A. Al-Yasari, P. Spence, H. El Moll, N. Van Steerteghem, P. N. Horton, B. S. Brunschwig, K. Clays, J. Fielden, *Dalton Trans.* 2018, **47**, 10415.

5. *CrysAlisPro* (Version 1.171.40.68a), Rigaku Oxford Diffraction, Rigaku Corporation, Tokyo, Japan, **2019**.

6. G. M. Sheldrick, *Acta Cryst. A*, **2015**, *71*, 3.

7. O. V. Dolomanov, L. J. Bourhis, R. J. Gildea, J. A. K. Howard, H. Puschmann, *J. Appl. Crysallogr.* **2009**, *42*, 339.

8. G. M. Sheldrick, *Acta. Cryst. C*, **2015**, *71*, 3.

9. S. K. Ibrahim, Ph.D Thesis, University of Sussex, **1992**.

10. J.D. Chai and M. Head-Gordon, *Phys. Chem. Chem. Phys.* **2008**, *10*, 6615.

12. A.D. Becke, *J. Chem. Phys*. **1997**, *107*, 8554.

13. R. Krishnan, J.S. Binkley, R. Seeger, J.A. Pople, *J. Chem. Phys.* **1980**, *72*, 650.

14. L.E. Roy, P.J. Hay, R.L. Martin, *J. Chem. Theory Comput.* **2008**, *4*, 1029.

15. E. Rtibi, M. Abderrabba, S. Ayadi, B. Champagne, *Inorg. Chem.* **2019**, *58*, 11210.

16. J. Tomasi, B. Mennucci, R. Cammi, *Chem. Rev*. **2005**, *105*, 2999.

17. M.E. Casida, in "Recent advances in Density Functional Theory", edited by D.P. Chong, Singapore, World Scientific (1995), pp 155-192.

18. T. Le Bahers, C. Adamo, I. Ciofini, *J. Chem. Theory Comput.* **2011**, *7*, 2498.

19. S.J.A. Van Gisbergen, J.G. Snijders, E.J. Baerends, *J. Chem. Phys*. **1998**, *109*, 10644.

20. T. Helgaker, S. Coriani, P. Jørgensen, K. Kristensen, J. Olsen, K. Ruud, *Chem. Rev.* **2012**, *112*, 543.

21. B. Champagne, P. Beaujean, M. de Wergifosse, M. Cardenuto, V. Liégeois, F. Castet, in Frontiers of Quantum Chemistry, edited by M. Wojcik, H. Nakatsuji, B. Kirtman, Y. Ozaki, Springer, Singapore, 2018, pp 117-138.

22. M. de Wergifosse, B. Champagne, *J. Chem. Phys.* **2011**, *134*, 074113.

23. L.E. Johnson, L.R. Dalton, B.H. Robinson, *Acc. Chem. Res*. **2014**, *47*, 3258.

24. K. Garrett, X.A. Sosa Vazquez, S.B. Egri, J. Wilmer, L.E. Johnson, B.H. Robinson, C.M. Isborn, *J. Chem. Theory Comput.* **2014**, *10*, 3821.

25. A. Tuer, S. Krouglov, R. Cisek, D. Tokarz, V. Barzda, *J. Comput. Chem.* **2011**, *32*, 1128.

26. J. Campo, W. Wenseleers, E. Goovaerts, M. Szablewski, G.H Cross. *J. Phys. Chem. C* **2008,** *112*, 287.

27. M. de Wergifosse, E. Botek, E. De Meulenaere, K. Clays, B. Champagne, J. *Phys. Chem. B* **2018**, *122*, 4993.

28. M.J. Frisch, G.W. Trucks, H.B. Schlegel, G.E. Scuseria, M.A. Robb, J.R. Cheeseman, G. Scalmani, V. Barone, G.A. Petersson, H. Nakatsuji, X. Li, M. Caricato, A. V Marenich, J. Bloino, B.G. Janesko, R. Gomperts, B. Mennucci, H.P. Hratchian, J. V Ortiz, A.F. Izmaylov, J.L. Sonnenberg, D.

Williams-Young, F. Ding, F. Lipparini, F. Egidi, J. Goings, B. Peng, A. Petrone, T. Henderson, D. Ranasinghe, V.G. Zakrzewski, J. Gao, N. Rega, G. Zheng, W. Liang, M. Hada, M. Ehara, K. Toyota, R. Fukuda, J. Hasegawa, M. Ishida, T. Nakajima, Y. Honda, O. Kitao, H. Nakai, T. Vreven, K. Throssell, J.A. Montgomery Jr., J.E. Peralta, F. Ogliaro, M.J. Bearpark, J.J. Heyd, E.N. Brothers, K.N. Kudin, V.N. Staroverov, T.A. Keith, R. Kobayashi, J. Normand, K. Raghavachari, A.P. Rendell, J.C. Burant, S.S. Iyengar, J. Tomasi, M. Cossi, J.M. Millam, M. Klene, C. Adamo, R. Cammi, J.W. Ochterski, R.L. Martin, K. Morokuma, O. Farkas, J.B. Foresman, D.J. Fox, Gaussian16 Revision A.03, **2016**.

29. DrawMol, V. Liégeois, U. Namur, www.unamur.be/drawmol.

30. F. Zutterman, V. Liégeois, B. Champagne, *ChemPhotoChem* **2017**, *1*, 281.

31. (a) K. Clays, A. Persoons, *Phys. Rev. Lett.* **1991**, *66*, 2980. (b) K. Clays, A. Persoons, *Rev. Sci. Instrum.* **1992**, *63*, 3285. (c) E. Hendrickx, K. Clays, A. Persoons, *Acc. Chem. Res.* **1998**, *31*, 675.

32. (a) G. Olbrechts, R. Strobbe, K. Clays, A. Persoons, *Rev. Sci. Instrum.* **1998**, *69*, 2233. (b) G. Olbrechts, K. Wostyn, K. Clays, A. Persoons, *Optics Lett.* **1999**, *24*, 403. (c) K. Clays, K. Wostyn, G. Olbrechts, A. Persoons, A. Watanabe, K. Nogi, X.-M. Duan, S. Okada, H. Oikawa, H. Nakanishi, H. Vogel, D. Beljonne, J.-L. Brédas, *J. Opt. Soc. Am. B* **2000**, *17*, 256. (d) E. Franz, E. C. Harper, B. J. Coe, P. Zahradnik, K. Clays, I. Asselberghs, *Proc. SPIE–Int. Soc. Opt. Eng.* **2008**, *6999*, 699923-1–699923-11.

33. J. Campo, F. Desmet, W. Wenseleers, E. Goovaerts, *Opt. Express* **2009**, *17*, 4587.